Egypt. J. Chem. **Vol. 68**, No. 8 pp. 613 -630 (2025)

Egyptian Journal of Chemistry

http://ejchem.journals.ekb.eg/

Kinetic and Variables Analysis for Photo-Fenton by Synthetic Fe^{3+} Doped TiO_2 Nanoparticles to Destroy Brilliant Dye Pollutants

Gamalat E. Mahmoud

Chemistry Department, Faculty of Science (Girls), Al-Azhar University Nasr City, Cairo, Egypt

Abstract

Reactive Red 12 (RR 12) dye, also known as Brilliant Red B dye, is a highly pigmented substance that contaminates wastewater when it's used to dye and print textiles. To stop the dopant cation from penetrating the bulk of TiO_2, Fe^{3+}doped TiO_2 composite nanoparticles (Fe^{3+} = 0.02 wt.%) were successfully synthesized using an incipient wet impregnation method. SEM, EDX, XRD, and TEM characterized the undoped TiO_2 and Fe^{3+}doped TiO_2 nanoparticles. Studies indicate that when Fe^{3+} is doped, the size of the Fe^{3+}doped TiO_2 particles decreases and their XRD peaks broaden. The transformation of TiO_2 from anatase to rutile can be regulated by doping Fe^{3+}. The oxidation of RR 12 is significantly enhanced by the photocatalytic and Photo-Fenton treatments that use Fe^{3+}doped TiO_2 nanoparticles in the presence of H_2O_2. The doping amount of Fe^{3+} remarkably affects the activity of the catalyst. Several factors, including Fe^{3+}doped TiO_2 catalyst dosage, pH, initial dye concentration, contact time, and H_2O_2 amounts, affect how quickly the dye is degraded.Langmuir and Freundlich's models of adsorption looked at the adsorption of RR 12. The Langmuir equation was found to fit more closely than the Freundlich equation.The kinetics of the adsorption at the different initial dye concentrations by pseudo-first order and pseudo-second order were also examined. According to the kinetic investigations, the adsorption kinetics were clarified by the pseudo-second-order kinetic model, which raised the possibility that chemisorption was the adsorption mechanism.

Keywords: Fe^{3+}Doped TiO_2 Nanoparticles, Kinetics, Isotherms, Photo-Fenton Treatments, Dye Pollutant.

1. Introduction

The contaminants found in wastewater from factories are colored pollutants, sometimes referred to as dyes. According to Khatri and colleagues [1] dyes used in textiles are extremely hazardous, mutagenic, and carcinogenic. Additionally, they decrease photosynthetic activity [2] and block light from entering water [3], reducing oxygen in water bodies. As a result, downstream uses like irrigation, drinking water supply, agriculture, and leisure are negatively impacted [4]. Water-soluble textile dyes are highly resistant to environmental conditions, including light, temperature, soap, sweat, chemicals, bleach, acid, alkali, and detergents. As a result, they never break down in the environment [5].

Reactive dyes have been the subject of much attention lately because of their wide availability and the requirement to manage water effluent so that it is disposed of after pretreatment. The motive for the focus is that these dyes, especially reactive dyes, have been found widely in water released from dyeing and printing facilities [6].This has led to the development of technologies for treating sewage from dyes and textiles, which include flocculation itself bleeding [7], and sophisticated procedures for oxidation [8], as well as membrane techniques [9], photocatalytic degradation [10], and electrical implementation. [11], living agent therapy [12], while adsorbing [13].

Advanced oxidation processes, or AOPs, are a type of chemical treatment that can convert pollutants into smaller, greener molecules. Because it is simple to use and has a powerful ability to oxidize under moderate reaction circumstances, the Fenton oxidation reaction is one of the AOPs capable of eliminating organic materials from wastewater. Nonetheless, exposure to light can enhance the system's catalytic activity. An essential procedure is the photo-Fenton reaction, which produces hydroxyl radicals with the $Fe^{2+}/H_2O_2/UV$ system. In the $Fe^{2+}/H_2O_2/UV$ system, water is a catalyst for releasing ferrous ions [14]. The "homogeneous photo-Fenton process" is the name of this method. A homogeneous Photo-Fenton process has certain drawbacks, though. After the reaction, iron ions can be challenging to separate and reuse. Therefore, the heterogeneous catalyst used in the Photo-Fenton process was intriguing since it is simpler to differentiate than the homogeneous catalyst following the reaction. Furthermore, one of the AOPs frequently employed in the restoration of water and air is the arrangement of titanium dioxide (TiO_2) as a photocatalyst. Moreover, the Photo-Fenton process can utilize the light source's energy. TiO_2 is a widely used photocatalyst due to its low toxicity, high photoactivity, chemical

*Corresponding author e-mail: gmalat@azhar.edu.eg.; (Gamalat Mahmoud).
Received Date: 20 November 2024, Revised Date: 15 December 2024, Accepted Date: 17 December 2024
DOI: 10.21608/EJCHEM.2024.337668.10841

stability, self-cleaning properties, narrow band gap, and affordability. The two primary mechanisms for reaction in the photocatalytic process are adsorption and photocatalytic reaction. TiO_2 is therefore a catalyst that can raise the adsorption rate and is advantageous to the photocatalytic process overall [15].

The current study investigates the usage of an AOP in the photocatalytic and Photo-Fenton processes, which break down the azo RR 12 dye using Fe^{3+}doped TiO_2 nanoparticles in the presence of H_2O_2. The impacts of Fe^{3+}doped TiO_2 nanoparticles and undoped TiO_2 Degussa P25 nanoparticles exposed to UV light at a wavelength of 254 nm will be compared in a laboratory setting photoreactor. RR 12 dye is now utilized in the paper and textile industries and is found in their wastewater, it was chosen as an intolerant emulation pollutant. SEM, EDX, TEM, and XRD were used to examine the morphological structure of the photocatalysts. Many other factors, including pH, Fe^{3+}doped TiO_2 catalyst dosage, contact time, initial dye concentration, and H_2O_2 amounts, affect how quickly RR 12 dye degrades. Using information from adsorption equilibrium and kinetics led to the discovery of RR 12 dye adsorption mechanism on Fe^{3+}doped TiO_2 nanoparticles.

2. Experimental

2.1. Chemicals

The German TiO_2 Degauss P25 (30 nm particle size) was employed as a photocatalyst. Reactive Red 12 (RR 12), also known as Brilliant Red B (Ciba-Geigy). The pH of the solution was adjusted using NaOH solutions (Panreac) and H_2SO_4 (Sigma Aldrich, 98%). $Fe(NO_3)_2{\cdot}6H_2O$ and H_2O_2 from Merk or BDH. Applying the chemicals exactly as received, none of the products were of the reagent grade. The composition and characteristics of the dye are shown in Table 1:

Table 1: Some physical attributes of Brilliant Red B.

Name	Molecular Structure	Molecular formula	Molecular weight (g/mol)	Wavelength, λ_{max} (nm)	Chemical Structure
C.I. Reactive Red 12, Brilliant Red B (RR 12)	Single azo class	C19H11ClN7 Na3O10S3	697.95	519	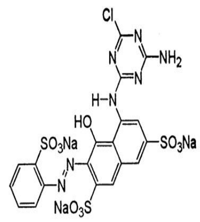

2.2. Solutions to stock dyes

A stock solution containing one milligram of (RR 12) dye per liter was created by dissolving one milligram of the dye into one thousand milliliters of double-distilled water as demonstrated in Figure 1. Double-distilled water is used to dilute the stock solution to make all solutions studied.

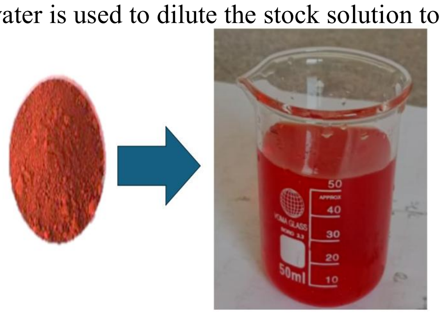

Figure 1:Powder (RR12) and stock solution.

2.3. Getting the Fe^{3+}doped TiO_2 Ready

Wet impregnation was used to prepare the Fe^{3+}doped TiO_2 catalyst to stop the dopant cations from penetrating the bulk of the material. This is because bulk doping speeds up the recombination rate of charge carriers, which lowers the catalyst's photocatalytic activity. A particular quantity of doubly distilled water was combined with 8g of TiO_2 Degussa P25 and the appropriate amount of $Fe(NO_3)_2{\cdot}6H_2O$, and the mixture was mixed thoroughly for one hour. Depending on the Fe concentration, the color of the mixture changed during this time to a light brownish beige. Four distinct Fe-doped photocatalysts are made with Fe^{3+}contents (Fe^{3+}= 0.01, 0.02, 0.04, and 0.06 wt.%). After that, the collected photocatalysts underwent three water washes, a heat treatment at 100 °C for 24 hours to remove water, a 4-hour calcination at 500 °C, grinding, and sieving [16]. This preparation is shown in Figure 2. Therefore, the only things examined in the present investigation are the characterization and photocatalytic activity of the doping content (Fe^{3+} = 0.02 wt.%).

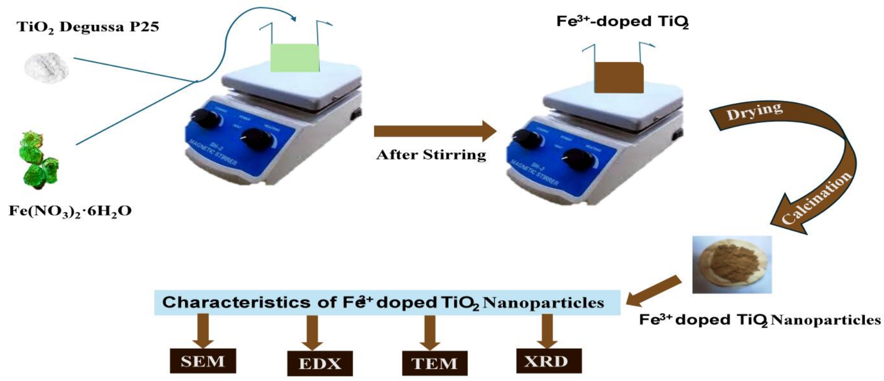

Figure 2: A schematic illustration of Fe^{3+}doped TiO_2nanoparticles.

2.4. Batch examines at balance

A 6WHg lighting (254 nm) was positioned in the middle of a 500 mL quartz catheter for the photocatalytic split of the RR 12 remedy (Figure 3). The bulb was placed inside a conical quartz case thathelps to evacuate heat and has a waterproof garment. 25 mL of RR 12 remedy with the photocatalyst (Fe^{3+}doped TiO_2) was added to a quartz catheter (Figure 3).

This research involves trials to determine the ideal operation conditions for RR 12 dye removal. To create varying amounts of RR 12, a stock solution was diluted using double-distilled water. Among the variables that were investigated (Fe^{3+}= 0.01–0.06 wt.%), Fe^{3+}doped TiO_2photocatalyst dosage, the (10 –180 mins) duration of contact, the concentration of H_2O_2 (0.00–25.00 mM), (1.10-9.30) pH, and the (9.77–69.79 mg/L) initial concentration of the RR 12 dye. The sample's pH value was then adjusted to the desired range utilizing both solutions, the (NaOH, 0.1 M) sodium hydroxide or (HCl, 0.1 M) hydrochloric acid, and (Model-CR.10P, DENVER CO., LTD) used as a pH reader. The mixture was then magnetically agitated in the dark for about 30 minutes to accomplish the adsorption of an equilibrium state before being exposedto radiation. After being exposed to ultraviolet rays, the reaction known as photocatalysis began. The specimens of RR 12 liquid were taken at set times and enacted within used only once,filtered for syringes to get rid of any last traces of catalyst fragments in the mixture. Using an ultraviolet (UV)-visible spectrophotometer (Modsel-303UV, APEL CO., LTD), the adhesion of the colorant solution was recognized to evaluate the functioning of the artificially produced photocatalyst. A curve for calibration built about analyses of the mentioned RR 12 remedy was used to establish a causal relationship between adsorption and dye memory. The RR 12 solution uses (UV)-visible absorbing spectroscopy to track it after the absorbance quantity readings at λ_{max}519 nm remained fixed [17]. (Equations. 1, 2, and 3) were used to ascertain (q_t), (q_e), the RR 12 proportion adsorbed when t and balance (mg RR 12 /g Fe^{3+}doped TiO_2 catalyst), and the degree of dye elimination capacity of RR 12 [18].

$$q_e = \frac{V}{W}(C_o - C_e) \quad \text{Eq. (1)}$$

$$q_t = \frac{V}{W}(C_o - C_t) \quad \text{Eq. (2)}$$

$$\%\ \text{dye elimination degree} = \left(\frac{C_o - C_e}{C_o}\right) x\ 100 \quad \text{Eq. (3)}$$

where V was the volume of the dye solution (l), W was the weight of the Fe^{3+}doped TiO_2 catalyst applied (g), C_o, C_e, and C_t are the initial, equilibrium, and at time t solution concentrations (mg/L), accordingly.

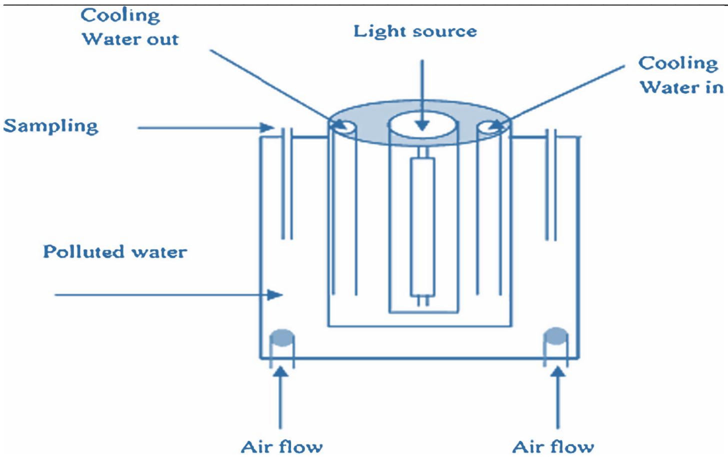

Figure 3: The architecture of the photoreactor.

2.5. The catalyst's (Fe^{3+}doped TiO_2) characteristics

The surface morphology of Fe^{3+}doped TiO_2 (Fe^{3+} = 0.02 weight percent) and TiO_2 Degussa P25 samples was examined using a JEOL SEM-25 scanning electron microscope. Before examination, the specimens were dried out under spray gold.

OXFORD link ISIS Energy Dispersive X-ray Spectroscopic was used to analyze the EDX pattern of TiO_2 Degussa P25 and Fe^{3+}doped TiO_2 (Fe^{3+}= 0.02 wt.%).

A JEM-100 CX (JEOL Ltd.) was used to analyze the TEM of TiO_2 Degussa P25 and Fe^{3+}doped TiO_2 (Fe^{3+}= 0.02 wt.%) measurements.

Using a contemporary Shimadzu Diffractometer x D-D1 Series, the X-ray diffraction patterns of TiO_2 Degussa P25 and Fe^{3+}doped TiO_2 (Fe^{3+}= 0.02 wt.%) samples were measured.

3. Results and discussion

3.1. Fe^{3+}doped TiO_2 and TiO_2 Degussa P25 characterizations

3.1.1. Fe^{3+}doped TiO_2 and TiO_2 Degussa P25 SEM morphologies

The SEM micrographs for the Fe^{3+}doped TiO_2 and TiO_2 Degussa P25 are displayed in Figure 4. TiO_2 Degussa P25 contains homogenous, regular, and polyhedral particles, as shown in Figure 4a. The Fe^{3+}doped TiO_2, on the other hand, has pointed corners and smaller particles with straight edges as shown in Figure 4b.

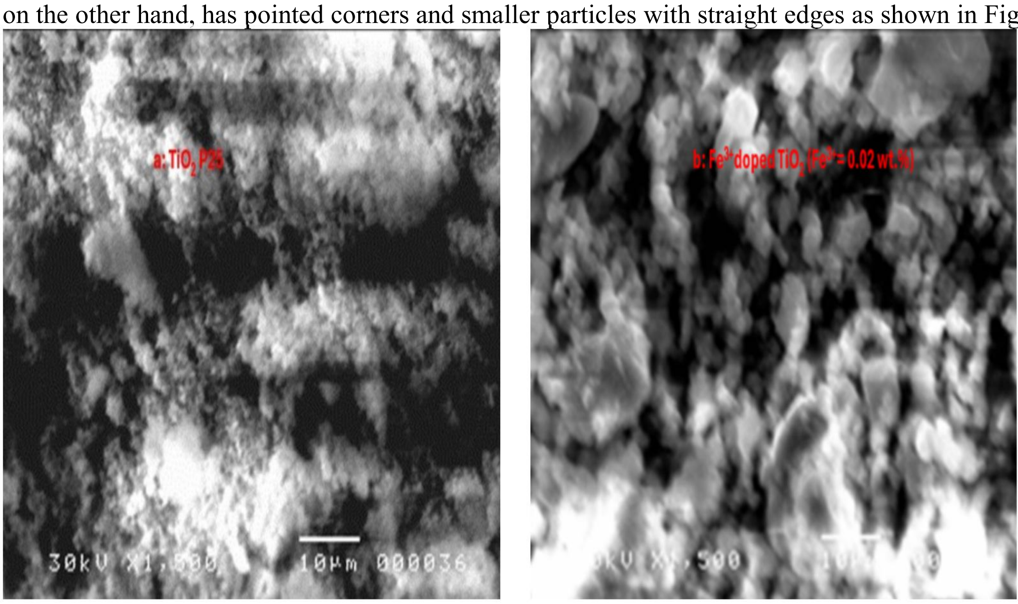

Figure 4: Micrographs taken with SEM of (a)TiO_2 Degussa P25 and (b) Fe^{3+}doped TiO_2.

3.1.2. Fe^{3+}doped TiO_2 and TiO_2 Degussa P25 EDX spectra

The EDX spectra of Fe^{3+}doped TiO_2 and TiO_2 Degussa P25 are displayed in Figure 5. The amount determined by EDX analysis agrees with the contents of doping. Additionally, an almost uniform distribution of Fe^{3+} cations between the particles is shown in the EDX results.

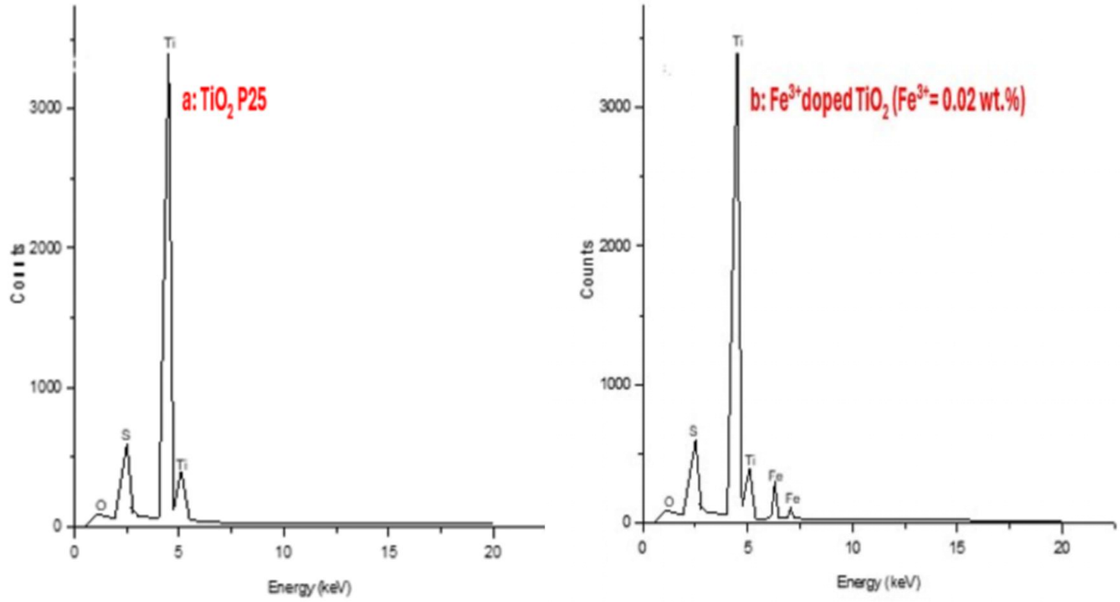

Figure 5: EDX spectrum of (a)TiO_2 Degussa P25 and (b) Fe^{3+}doped TiO_2.

3.1.3. TEM of Fe^{3+}doped TiO_2 and TiO_2 Degussa P25

The TEM of TiO_2 Degussa P25 and Fe^{3+}doped TiO_2 is displayed in Figure 6. The average particle sizes for their two types of materials are 40.3 and 33.7 (nm), respectively. The sizes decrease as the Fe^{3+} content increases. These findings show that Fe^{3+} doping inhibits the growth of the TiO_2 crystal grains, leading to a reduction in particle size [19] and an elevation of surface energy, which could lead to crystal grain accumulation.

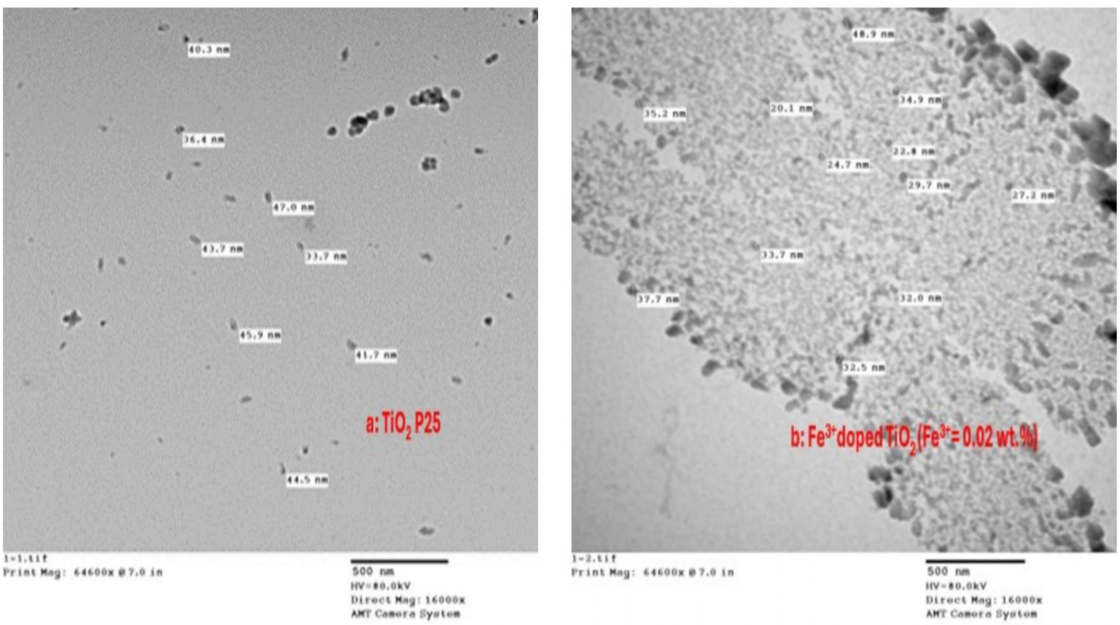

Figure 6: TEM imagery of (a)TiO_2 Degussa P25 and (b) Fe^{3+}doped TiO_2.

3.1.4. XRD analysis of TiO_2 Degussa P25 and Fe^{3+}doped TiO_2

An X-ray diffractometer was used to evaluate the Fe^{3+}doped TiO_2 catalyst to ascertain its degree of crystallinity and pinpoint the metal ions, Fe^{3+}, doped on TiO_2. Fe/TiO_2 diffraction patterns from X-rays are displayed in Figure 7. Anatase and rutile phases can both be seen in Figure 7(a). Both phases have molar proportions of 21% rutile and 79% anatase. The diffractions of the (101), (004), and (200) anatase-type TiO_2 are explained by the peaks at 2θ 25.31, 37.81, and 48.01, as illustrated in Figure 7a, with the main XRD diffractogram located at 25.31. At 2θ 27.51, rutile TiO_2 exhibits a distinctive peak [20]. Figure 7(b) illustrates how (1) the anatase to rutile transformation is catalyzed by iron, resulting in the detection of rutile. These findings show that the doping Fe^{3+} controls the crystalline conversion of TiO_2 from the rutile to the anatase phase. The peak areas of diffraction are noticeably enlarged. Grain size and crystal defects are two examples that influence the broadening of diffraction peaks.

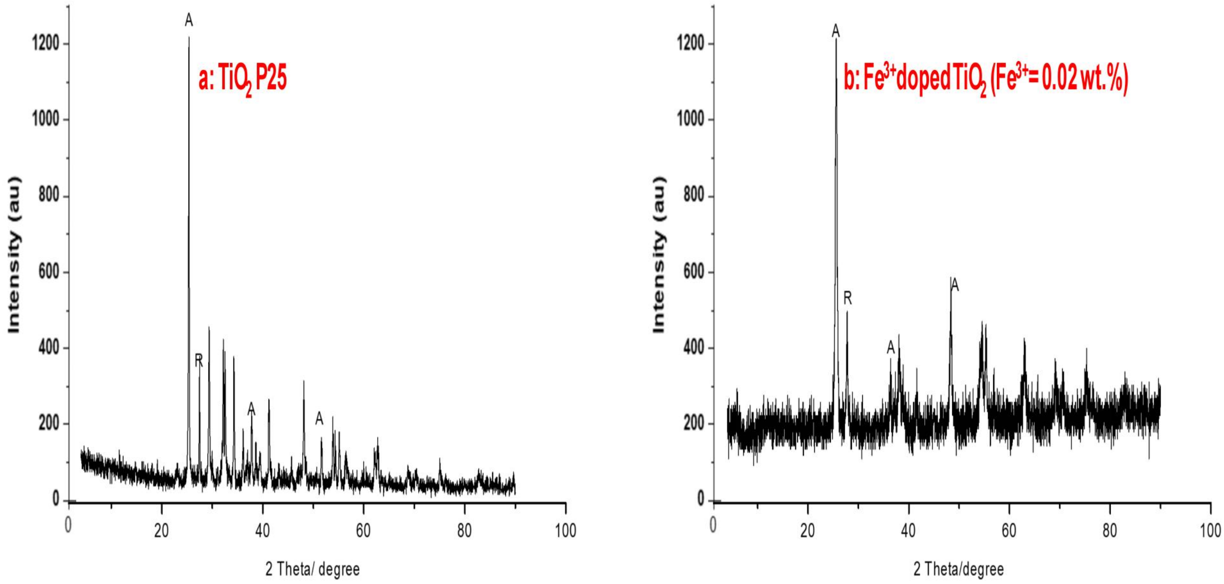

Figure 7: (XRD), diffractograms of (a)TiO_2 Degussa P25 and (b) Fe^{3+}doped TiO_2, where A: anatase and R: rutile.

3.2. Variables influencing the Fe^{3+}doped TiO_2 photocatalytic degeneration of RR 12

The Fe^{3+}doped TiO_2catalyst was chosen for its ability to be utilized in the degradation of RR 12 through the Photo-Fenton oxidation reaction. Numerous factors were discovered to influence the Photo-Fenton oxidation reaction's efficiency, including the dosage of the Fe^{3+}doped TiO_2catalyst, pH, initial dye concentration, contact time, and amounts of H_2O_2.

3.2.1. Effect of undoped TiO_2-P25 and Fe^{3+}doped TiO_2 catalyst dosage

RR 12's photocatalytic mechanism was examined by adsorbing undoped TiO_2 and Fe^{3+}doped TiO_2nanoparticles. After 30 minutes, the dark experiment shows a decrease in absorbance at λ_{max} 519nm of more than 33%, which suggests that RR 12 has been adsorbed onto both Fe^{3+}doped $TiO_2$and undoped TiO_2 surfaces. The photodegradation of RR 12 by using UV-irradiation within time (180 mins) at fixed dye concentration (9.77 mg/L), H_2O_2 concentration (10 mM), and pH 3.50 were evaluated using 0.50 g/l of undoped TiO_2-P25 alone and compared with 0.50 g/l of different concentrations of Fe^{3+}doped TiO_2(Fe^{3+}= 0.01, 0.02, 0.04, and 0.06 wt.%). These experiments examine the potential for concurrent photodegradation of RR 12 when adsorbed onto surfaces of Fe^{3+}doped $TiO_2$and undoped TiO_2. In comparison to photodecolorization in the presence of undoped TiO_2-P25, which achieves 60.66% at the same time, 99.69% of the red color of the RR 12 solution vanished after 50 minutes of photodecolorization in the presence of Fe^{3+}doped TiO_2. The degree to which RR 12 can be eliminated by radiation in the presence of Fe^{3+}doped $TiO_2$and TiO_2-P25 is demonstrated in Figure 8. Because of this, the results for the Fe^{3+}doped TiO_2catalyst that are being given indicate the ideal dose (Fe^{3+}= 0.02 wt.%), which corresponds to the optimum absorption of light. When Fe^{3+} is doped to a level of 0.02 weight percent, photocatalytic activity rises and subsequently falls with the other doping levels.

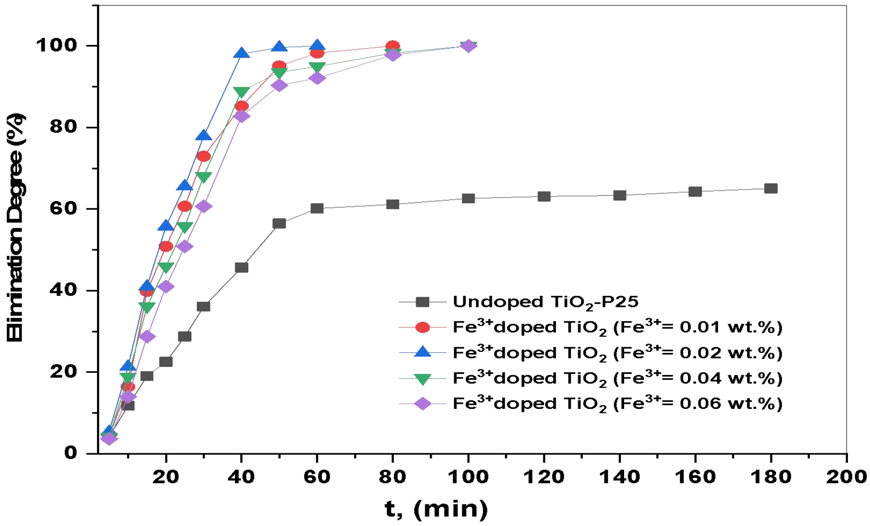

Figure 8: The degree of elimination of RR 12 atthe impact of the initial catalyst (Fe^{3+}doped TiO_2) dosage.

Data in Figure 9 shows that the Fe^{3+}doped TiO_2 sample expressed higher initial activities than that of undoped TiO_2 P25. The electron or hole traps and metal ion doping affect the photoactivity of TiO_2. Dopant beginning works well because the trap can generate some active species that aid in dye degradation. More photo-generated electrons and holes are produced to participate in the photocatalytic processes as an outcome of Fe^{3+} ions' strong absorption in the UV–visible light region and red shift in the Fe^{3+}doped TiO_2 spectrum shift. The result is comparable to that of Zhu et al. [21], who noticed that photogenerated electrons on the conduction band of TiO_2 could transfer to the catalyst's surface, inhibiting electron-hole pair recombination and increasing the utilization of holes on TiO_2. Furthermore, the conduction band of TiO_2 is more negative than the $O_2/O^{\bullet-}{}_2$ potential (−0.046 V vs. NHE) [22], suggesting that the heterogeneous Fenton reaction can produce $O^{\bullet-}{}_2$ from photogenerated reaction electrons with O_2. Both $O^{\bullet-}{}_2$ and $^{\bullet}OH$ can participate in the breakdown of RR 12. Consequently, the Fe^{3+}doped TiO_2 catalyst can degrade RR 12 more efficiently than Fe^{2+} (the traditional heterogeneous Fenton catalyst) and TiO_2 (the conventional semiconductor). The reaction response may be shown as follows in Equations 4- 6:

$TiO_2 + hv \rightarrow TiO_2\,(h^+_{VB} + e^-_{CB})$ Eq. (4)

$Fe^{3+} + e^-_{CB} \rightarrow Fe^{2+}$ Eq. (5)

$Fe^{2+} + O_2 \rightarrow Fe^{3+} + O_2^{-\bullet}$ Eq. (6)

Additionally, it may speed up the reduction of Fe(III) to Fe(II) on the surface, the Fenton reaction, which occurs when Fe^{2+} and H_2O_2 coexist in acidic media, resulting in enhanced H_2O_2 breakdown and $^{\bullet}OH$ production. Furthermore, $^{\bullet}OH/H_2O$ has a lower potential for redox reactions (2.27 V vs. NHE) than OH^- and H_2O, which can be oxidized to $^{\bullet}OH$ shown in Equation 7 [23]. Subsequently, the RR 12 will undergo an oxidation reaction with the $^{\bullet}OH$.

$Fe^{2+} + H_2O_2 + H^+ \rightarrow Fe^{3+} + HO^{\bullet} + OH^-$Eq. (7)

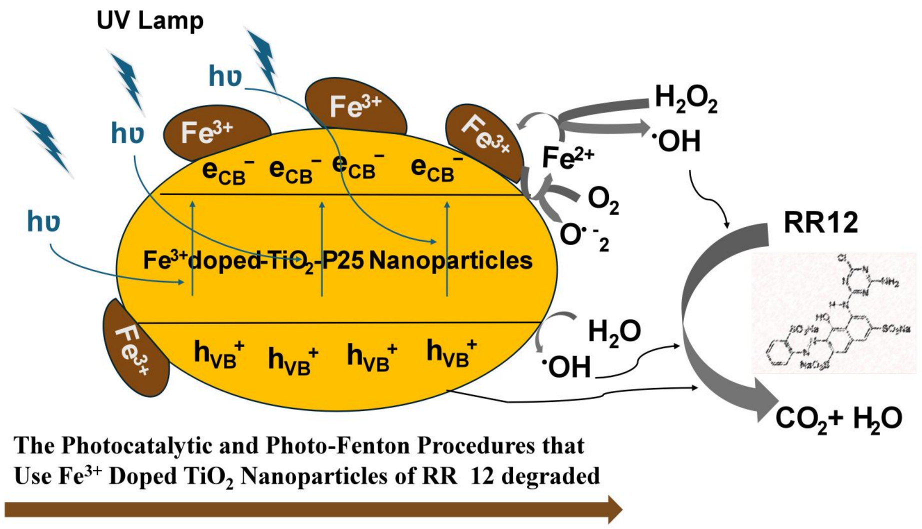

Figure 9: A schema showing the photocatalytic and photo-Fenton mechanism of the doped TiO_2 nanoparticles in the breakdown of RR 12 by using UV irradiation.

Furthermore, the Langmuir–Hinshelwood equation, which additionally addresses the substrate's adsorption characteristics on the photocatalyst surface, is frequently used to model the photocatalytic degradation kinetics of a variety of organic compounds, the rate equation is reduced to a pseudo-first-order rate equation concerning the dye concentration when the initial dye concentrations are relatively low [24]. This is represented by Equations (8, and 9):

$-Ln\frac{C_t}{C_o} = k_{app}t$Eq. (8)

$t_{1/2} = \frac{Ln\,2}{k_{app}}$Eq. (9)

C_o, C_t, and k_{app} are the initial concentration and concentration at time t, respectively, and the degradation is the apparent rate constant. The concentration of RR 12 in the presence of various catalysts versus irradiation time produced semi-logarithmic graphs that gave straight lines that passed through the origin, signifying a pseudo-first-order reaction. The prominent reaction rate constants (k_{app}) for the photocatalytic degradation of RR 12 are calculated using linear regression based on experimental data. The correlation coefficient, or R^2, values are consistently greater than 0.98, indicating that dye decolorization kinetics in this procedure are valid. Figure 10 and Table 2 list the estimated prominent reaction rate constants (k_{app}) and half-life time of the photocatalytic degradation of RR 12. Table 2's data demonstrates the presence of Fe^{3+}doped TiO_2 (Fe^{3+}= 0.02 wt.%), the computed rate constant for RR 12 photodegradation is 35.80x $10^{-3}min^{-1}$. As anticipated, the Fe^{3+}doped TiO_2nanoparticles exhibit improved photocatalytic properties as opposed to the pure TiO_2-P25 photocatalyst ($12.40x10^{-3}min^{-1}$).

Table 2: The measurements of $R_{initial}$ ($gL^{-1}min^{-1}$), $t_{1/2}$ (min), and k_{app} (min^{-1}) for photocatalytic RR 12 elimination at various initial catalyst (Fe^{3+}doped TiO_2) dosages.

Parameter / Catalyst Dosage	k_{app} x10^3 (min^{-1})	$t_{1/2}$ (min)	$R_{initial}$ x 10^4 (k_{app} x C_0) ($gL^{-1}min^{-1}$)	R^2
1. Undoped TiO_2-P25	12.40	55.71	1.21	0.981
2. Fe^{3+}doped TiO_2 (Fe^{3+}= 0.01 wt.%)	29.80	23.20	2.91	0.991
3. Fe^{3+}doped TiO_2 (Fe^{3+}= 0.02 wt.%)	35.80	19.36	3.49	0.992
4.Fe^{3+}doped TiO_2 (Fe^{3+}= 0.04 wt.%)	25.60	27.07	2.50	0.985
5. Fe^{3+}doped TiO_2 (Fe^{3+}= 0.06 wt.%)	21.80	31.79	2.13	0.981

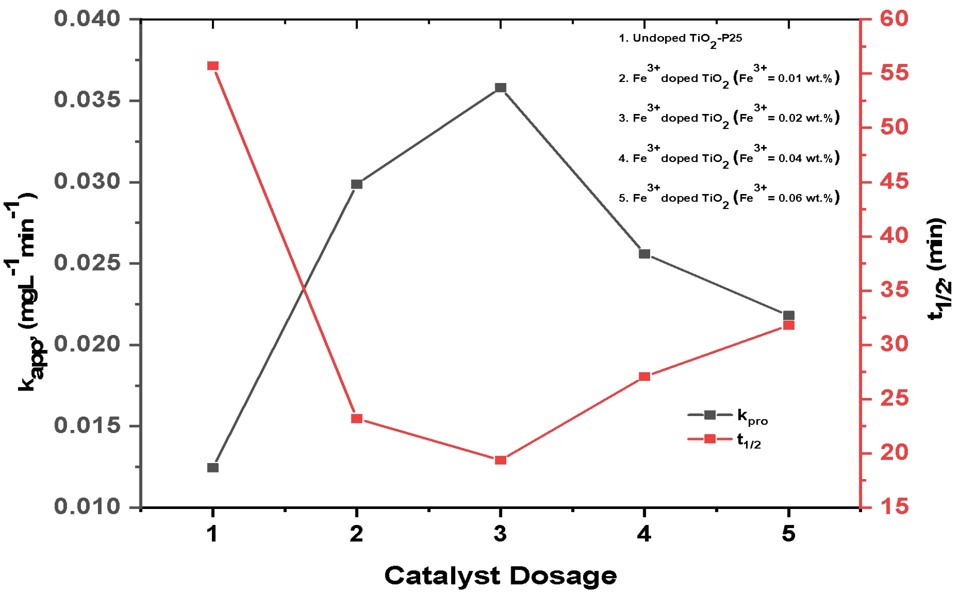

Figure 10: Demonstrate the impacts of catalyst (Fe^{3+}doped TiO_2) dosages on the RR 12 photodegradation apparent rate constant (k_{app}) and half-life time ($t_{1/2}$).

3.2.2. Impact of concentration of H_2O_2

RR 12's photocatalytic disintegration was investigated at various concentrations of hydrogen peroxide. On the photodegradation of RR 12 exposed to UV light within time (60 min) at set dye concentration (9.77 mg/L) and pH 3.50, the impact of changing the initial H_2O_2 concentration (0.00 – 25.00 mM) with 0.50 g/L from Fe^{3+}doped TiO_2 catalyst (Fe^{3+}= 0.02 wt.%) has been investigated. The elimination degree of RR 12 gives a higher value for a 10 mM concentration of H_2O_2 (99.99 %) beyond this point, it falls (Table 3). The photocatalytic reactivity is controlled by the Langmuir–Hinshelwood system [24].Overall, a strong correlation is found, indicating a pseudo-first-order rate law governs the reaction kinetics. The apparent rate constants (k_{app}), shown in Table 3, are obtained from the slopes of the straight lines that pass through the origin. Up to 10 mM, the degradation rate of RR 12 increases as the concentration of H_2O_2 rises; beyond this point, the degradation rate falls. As a result, adding hydrogen peroxide appropriately could quicken RR 12's photodegradation rate.

Yet the right quantity of hydrogen peroxide must be selected from the types and concentrations of pollutants to maintain the effectiveness of the added hydrogen peroxide. As a result of all the catalysts examined, RR 12 degraded the slowest with (0 mM) H_2O_2. This is considering UV light itself gradually absorbed in the absence of H_2O_2. When the Fe^{3+}doped TiO_2 catalyst is exposed to UV light and H_2O_2 (Figure 11), the rate of RR 12 degradation is high. This is probably due to the system's higher yield of $^{\bullet}OH$ [25]. The reaction response may be shown as follows (Equations (10-12)):

$2e^-_{CB} + H_2O_2 \rightarrow HO^{\bullet} + OH^-$ Eq. (10)

$O_2^{-\bullet} + H_2O_2 \rightarrow HO^{\bullet} + OH^- + O_2$ Eq. (11)

$H_2O_2 + h\upsilon \rightarrow 2HO^{\bullet}$ Eq. (12)

When hydrogen peroxide adheres to a high concentration on the photocatalytic surface, it can efficiently scavenge the photo-generated holes (h_{CB}^+) (Equation 13) and the $^{\bullet}OH$ radicals created on the surface (Equations 14 and 15). This inhibits the primary process, leading to the heterogeneous generation of $^{\bullet}OH$ radicals.

$HO^{\bullet} + H_2O_2 \rightarrow H_2O + HO_2^{-\bullet}$ Eq. (13)

$HO^{\bullet} + HO_2^{-\bullet} \rightarrow H_2O + O_2$ Eq. (14)

$h^+_{VB} + H_2O_2 \rightarrow H^+ + HO_2^{-\bullet}$ Eq.(15)

Table 3: The measurements of $R_{initial}$ ($gL^{-1}min^{-1}$), $t_{1/2}$ (min), k_{app} (min^{-1}) and E.D. (%) for photocatalytic RR 12 elimination at various amounts of H_2O_2.

H_2O_2 Conc. (mM)	Parameter				
	k_{app} x10^3 (min^{-1})	$t_{1/2}$ (min)	$R_{initial}$ x 10^4 (k_{app} x C_0) ($gL^{-1}min^{-1}$)	R^2	E.D. (%)
0	4.40	157.53	0.43	0.964	45.77
5	19.00	36.48	1.85	0.971	89.22
10	35.80	19.36	3.49	0.997	99.99
15	25.60	27.07	2.50	0.991	98.01
20	22.80	30.40	2.23	0.985	93.45
25	20.80	33.32	2.03	0.977	90.35

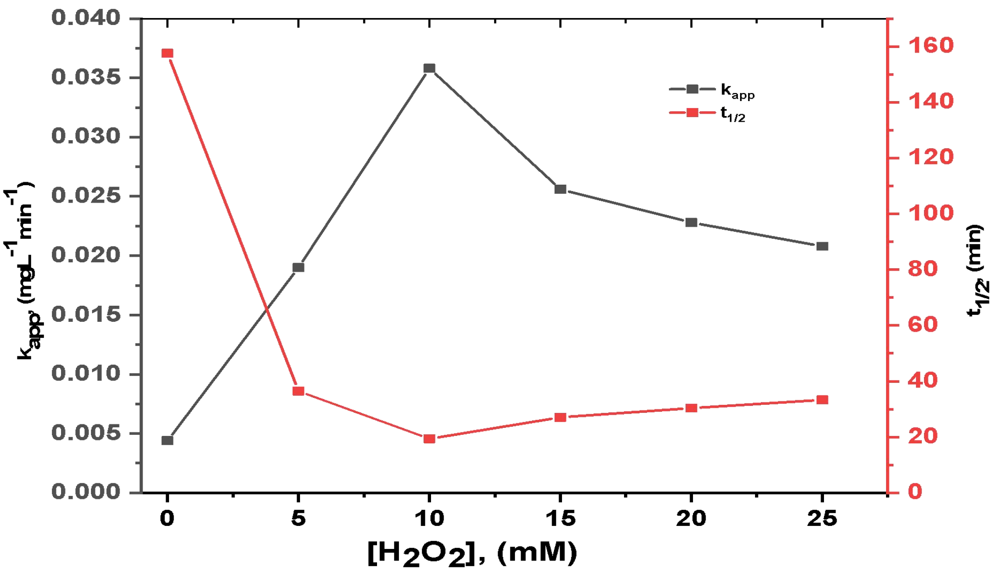

Figure 11: Demonstrate the impacts of various amounts of H_2O_2 on the RR 12 photodegradation apparent rate constant (k_{app}) and half-life time ($t_{1/2}$).

3. 2. 3. Effect of pH

The photodegradation of RR 12 at set dye concentration (9.77 mg/L) and H_2O_2 concentration (10 mM) has been tested, as has the photocatalytic decomposition of RR 12 at different pH values (pH = 1.1-9.3) with 0.5 g/L from Fe^{3+}doped TiO_2 catalyst (Fe^{3+}= 0.02 wt.%) within 60 minutes of UV-radiation exposure. The elimination degree of RR 12 gives a higher value for a pH = 3.50 (E.D. = 99.99 %) beyond this point, it falls and then reaches pH = 7.00 (E.D. = 40.45 %) after this point increase in alkaline medium (Table 4).

The photocatalytic reactivity is controlled by the Langmuir–Hinshelwood system [24]. Overall, a strong correlation is found, indicating a pseudo-first-order rate law governs the reaction kinetics. The (k_{app})apparent rate constants, shown in Table 4, are obtained from the slopes of the straight lines that pass through the origin. Figure 12 and Table 4 list the (k_{app})estimated prominent reaction rate constants and half-life time of the photocatalytic degradation of RR 12 at variouspH.

According to the findings in Table 4, raising the dye solution pH (1.1 − 3.50) results in an increase in the calculated rate constant (11.94 − 35.80 x 10^{-3} min^{-1}) during 60 minutes of receiving radiation. When the pH reaches 7.00, the computed rate constant drops to 7.70 x 10^{-3} min^{-1}. In a pH = 9.05 alkaline medium, the degree of degradation rises to 9.18 x 10^{-3} min^{-1}.

Table 4: The measurements of $R_{initial}$ ($gL^{-1}min^{-1}$), $t_{1/2}$ (min), k_{app} (min^{-1}), and E.D. (%) for photocatalytic RR 12 elimination at impacts of pH.

pH	Parameter				
	k_{app} x10^3 (min^{-1})	$t_{1/2}$ (min)	$R_{initial}$ x 10^4 (k_{app} x C_0) ($gL^{-1}min^{-1}$)	R^2	E.D. (%)
1.50	11.94	63.33	1.06	0.964	65.08
2.40	21.87	31.69	2.13	0.971	88.22
3.50	35.80	19.36	3.49	0.997	99.99
5.01	16.00	43.32	1.56	0.951	75.55
6.04	10.00	69.31	0.97	0.945	60.11
7.00	7.70	90.01	0.75	0.937	40.45
9.05	9.18	75.50	0.89	0.941	60.22

The essential function of the solution pH plays in a semiconductor photocatalysis's ecological uses was covered by Hoffmann et al. [26]. Furthermore, Fujishima and Zhang [27] stressed how important pH affects titanium dioxide photocatalysis. relates to the surface's ionization process initially. Titanium dioxide has a point of zero charge (pzc) of pH 6.5. In an acidic solution, the pH is lower than pzc, and the Fe^{3+}doped TiO_2 surface is positively charged (Equation 16).

pH < pzc : Fe^{3+}doped $Ti-OH+H^{+} \rightarrow Fe^{3+}$doped $TiOH_2^{+}$Eq. (16)

The surface in the basic solution has a negative charge, as shown by the equation below (Equation 17):

pH > pzc: Fe^{3+}doped $Ti-OH+HO^{-} \rightarrow Fe^{3+}$doped $TiO^{-}+H_2O$Eq. (17)

The rate at which RR 12 degrades enhances as pH drops (pH= 3.50). Due to an electrostatic attraction between the anionic dye and the positively charged Fe^{3+}doped TiO_2 catalyst, significant adsorption to the anionic dye is seen on the Fe^{3+}doped TiO_2 particles at pH <6. Since dye molecules have a negative charge in alkaline solutions at pH >6.8, an increase in the density of Fe^{3+}doped TiO_2- groups on the semiconductor surface to the impact on dye molecular adsorption. An essential component of photocatalytic operations, the surface charge is determined by the electrical potential difference between the surface of a catalyst and its environment. The pH of the medium directly affects this potential difference, which is shaped by hydroxyl groups on the catalyst surface and eventually decides the optical properties of the solution [28]. To accurately determine the impact of pH on the photoactivity of the synthesis of Fe^{3+}doped TiO_2 nanocomposite, RR 12 was employed as an anionic dye in this context. Table 4 presents an illustration of the outcomes of the experiment. Higher RR 12 degradation efficiency was noted in acidic pH conditions. In line with established trends in photocatalysis, organic wastes are more readily degraded at pH levels that are acidic than at alkaline.

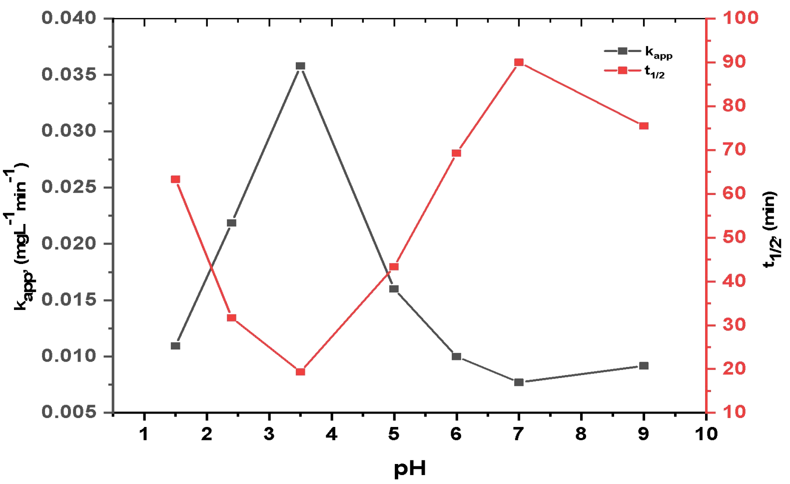

Figure 12: Demonstrate the impacts of pH on the RR 12 photodegradation apparent rate constant (k_{app}) and half-life time ($t_{1/2}$).

3.2.4. Impact of the starting concentration of dye

Studying how the photocatalytic degradation rate depends on the concentration of substrate (C_o) is necessary for the effective use of photocatalytic oxidation systems [29, 30]. The photodegradation of RR 12 under 60 minutes of UV light irradiation at pH=3.50 was examined and checked for the impact of initial dye concentrations (9.77–69.79 mg/L) with 0.50 g/L ofFe^{3+}doped TiO_2 catalyst (Fe^{3+}= 0.02 wt.%), and H_2O_2 concentration (10 mM). After 30 minutes, the dark test decreases the degradation degree calculated at λmax 519 nm, suggesting that the dye has been adsorbed at Fe^{3+}doped TiO_2 substrates. The elimination degree of RR 12 gives a higher value at a low initial dye concentration (9.77 mg/L) (E.D. = 99.99 %), beyond this point as the substrate concentration increased (Table 5).

Furthermore, as the concentration rises, the initial rate of photodegradation falls from its high value in the lower concentration range (Figure 13). The photocatalytic reaction typically proceeds as follows: The mechanism of Langmuir-Hinshelwood [24]. A strong correlation is found at low concentrations, indicating that a pseudo-first-order rate law governs kinetics. The apparent rate constants (k_{app}), shown in Table (5), are obtained from the slopes of the straight lines that pass through the origin. Numerous studies have shown that an increasing number of compound molecules are adsorbed on the surface of the photocatalyst when the concentration of the target contaminants rises. Thus, the $^{\bullet}OH$ and $O^{\bullet -}_2$reactive species needed for the pollutant to degrade likewise rise. On the other hand, for any specific light intensity, catalyst amount, and irradiation time, the creation of $^{\bullet}OH$ and $O^{\bullet -}_2$ on the catalyst surface stays constant. At higher concentrations of contaminants, the available $^{\bullet}OH$ is insufficient for their degradation. Furthermore, a rise in the concentration of the substance results in the production of intermediates that could potentially adsorb on the catalyst's surface. Deactivation of the photocatalyst's active sites and a decrease in the degradation rate can occur from the generated intermediates' gradual diffusion of the catalyst surface [31].

Table 5: The measurements of $R_{initial}$ ($gL^{-1}min^{-1}$), $t_{1/2}$ (min), k_{app} (min^{-1}), and E.D. (%) for photocatalytic RR 12 elimination at initial RR 12 concentrations.

RR 12 Conc. (mg/L)	Parameter				
	k_{app} x10^3 (min^{-1})	$t_{1/2}$ (min)	$R_{initial}$ x 10^4 (k_{app} x C_0) ($gL^{-1}min^{-1}$)	R^2	E.D. (%)
69.79	9.00	77.01	0.87	0.917	67.86
48.85	11.21	61.83	1.09	0.932	76.63
34.89	14.00	49.51	1.36	0.941	80.21
20.93	20.00	34.65	1.95	0.965	90.21
9.77	35.80	19.36	3.49	0.991	99.99

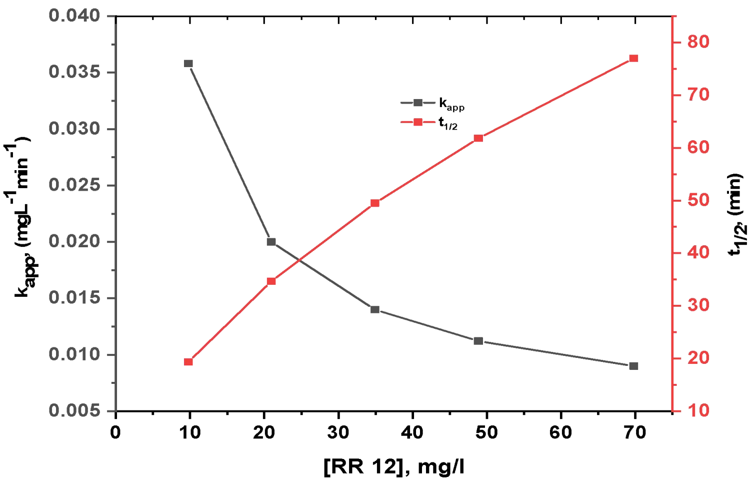

Figure 13: Demonstrate the effects of the initial RR 12 concentration on the RR 12 photodegradation apparent rate constant (k_{app}) and half-life time ($t_{1/2}$).

3.3. Examining RR 12 adsorption on the surface of Fe^{3+}doped TiO_2

It is important and relevant that RR 12 absorbs upon Fe^{3+}doped TiO_2 nanoparticles using a solution of water. For this reason, darkroom adsorption of Fe^{3+}doped TiO_2 nanoparticles is investigated. Most of the nanoparticle adsorption has been shown to occur in thirty minutes.

3.3.1. Consequences of contact time

The effect of contact time (equilibrium time) on RR 12 adsorption onto Fe^{3+}doped TiO_2 nanomaterial was investigated. (30 min), For RR 12 as shown in Figure 14, the speed of elimination was rapid during the initial short amount of time in engagement, but progressively decreased until the equilibrium period was attained. The electrostatic interaction between the RR 12 and the sites of activity on the Fe^{3+}doped TiO_2 is what causes the rapid state of equilibrium. Furthermore, the contaminants in organic colorants were easily able to access the mesoporous Fe^{3+}doped TiO_2due to its wide area of coverage [32].

The amount of RR 12 dye absorbed per g of (mg/g Fe^{3+}doped TiO_2) Fe^{3+}doped TiO_2 at all times is plotted versus contact (t) time in Figure 14. It is found that the capacity for adsorption increases in proportion to the starting concentration of RR 12. As the initial dye concentration rose, more dye was adsorbed onto Fe^{3+}doped TiO_2. As the initial dye concentration increases, it can be due to an increase in the power that drives the gradient of concentration [33]. This implies that the adsorption capability of RR 12 onto Fe^{3+}doped $TiO_2$is strongly influenced by the starting dye concentration.

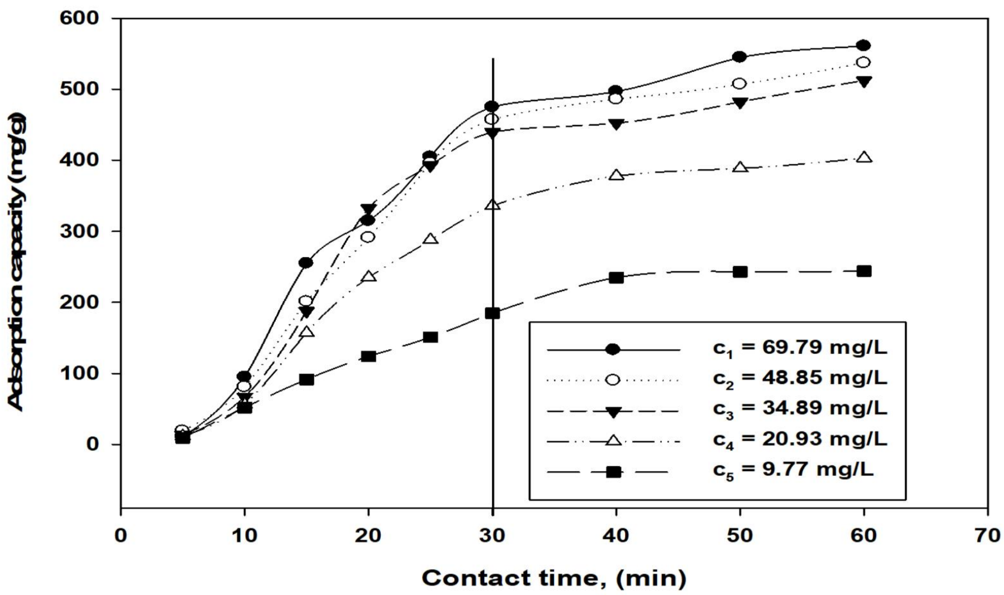

Figure (14): RR 12's adsorption onto Fe^{3+}doped TiO_2 nanoparticles at different amounts of dye and the effect upon contact period.

3.3.2. Isotherms of adsorption

Identification of adsorbate-adsorbent connections is facilitated through the knowledge obtained from studying adsorption at equilibrium. The equilibrium concentrations for adsorbate in liquid phase C and the solid phase q at a fixed temperature show adsorption isotherms [34]. The numerous mathematical methods used to express adsorption isotherms. Batch procedures are commonly used in laboratories to get equilibrium data, and different isotherm models, including Langmuir and Freundlich isotherms, are used to clarify the data [35].

3.3.2.1. The Isotherm of Langmuirtype

The Langmuir isotherm, which is successfully applied in many real sorb techniques, can be utilized to clarify the absorption of RR 12 over Fe^{3+}doped TiO_2. The Langmuir hypothesis states simply that absorption takes place within an adsorbent [34]. If places for adsorption are available, the Langmuir isotherm shows that adsorption increases as concentrated quantities grow. Once each area has been utilized, the level of saturation has been attained; any extra growth in the adsorbate fraction will not increase the amount adsorbed. The commonly employed two-parameter equation for the adsorption procedure (Equation 18) is used linearly [36]:

$$\frac{C_e}{q_e} = \frac{1}{Q_{max}K_L} + \frac{C_e}{Q_{max}} \quad \text{Eq. (18)}$$

where (q_e) is the amount of dye adsorbed per gram of Fe^{3+}doped TiO_2 (mg/g), (K_L) is the Langmuir constant (L/mg), which relates to the need for binding places, and (Q_{max}) is the estimated saturating capability of the monolayer (mg/g). (C_e) represents the dye concentration in the fluid at equilibrium (mg/l). The amounts of (Q_{max}) and (K_L) are obtained from the intercept as well as the slope of the linear graph of C_e/q_e to C_e (Figure 15a). The dimensionless separating factor, R_L, can be used to explain the fundamental properties of the Langmuir equation (Equation 19).

$$R_L = \frac{1}{1+K_L C_o} \quad \text{Eq. (19)}$$

where (C_o). denotes the RR 12's starting concentration. The (R_L) number indicates the following types of adsorption: Good: $0< R_L<1$; Irreversible: $R_L=0$; Poor: $R_L>1$; and A linear: $R_L=1$.

For all initial amounts, the correction coefficient (R^2), and the Langmuir isotherm constants, Table 6 shows a good: 0 < RL< 1 value. According to the Langmuir isotherm, our results show that RR 12 adsorbs onto Fe^{3+}doped TiO_2nanoparticles. The quantity of (Q_{max}) represents an acceptable limitation on adsorption capacity and helps with the adsorption comparison effectiveness if the surface is completely covered in dye molecules.

3.3.2.2. The Isotherm of Freundlich type

Also, the Freundlich model is a mathematical formula that assumes heterogeneous adsorption since the locations of adsorption differ. Equation 20 (the Freundlich equation) is [37]:

$$Ln\ q_e = Ln\ K_F + \frac{1}{n} Ln\ C_e \quad \text{Eq. (20)}$$

where K_F [mg/g (L/mg)1/n] approximately depicts the force of the adsorptive bonding, C_e is the equilibrium level of the dye concentration in liquid (mg/L), and Q_f and n are the Freundlich constants, which serve to measure the adsorption power and ability, respectively.(K_F) and (1/n) can be determined using the intercept and slope of a linear chart of Ln (qe) against Ln (C_e), as indicated in Figure 15b and Table 6. According to these findings, the use of the Freundlich formula was inappropriate since the correlation coefficient, R^2, is small (0.966) and the n value is greater than unity, signifying unfavorable adsorption.

Table 6: Features of RR 12 adsorption by Fe^{3+}doped TiO_2 nanoparticles as determined by Langmuir and Freundlich Isotherms.

IsothermsComparison							
Langmuir					Freundlich		
K_L (L/mg) (l/mg)	Q_{max} (mg/g)	C_o mg/L	R_L	R^2	n_F (g/L)	K_F (mg/g)	R^2
0.040	909.09	69.79	0.26	0.990	1.75	66.68	0.966
		48.85	0.33				
		34.89	0.41				
		20.93	0.54				
		9.77	0.71				

3.4. Adsorption kinetics

Combining pseudo-first- and pseudo-second-order approaches, modelling describing the experimental information were developed with a better understanding of the governing mechanism of the procedure of adsorption [38, 39].

3.4.1. Kinetic model of the first order

The kinematics of adsorbed information was analyzed to understand the motion of the method of adsorption concerning the ordering of the rate constant. Data from kinetics are subjected to the pseudo-first-order kinetic notion founded on tight capacities. Equation 21 for the rate of the pseudo-first-order equation [40]:

$$Ln\ (q_e - q_t) = Lnq_e - k_1 t \quad \text{Eq. (21)}$$

where (q_e) and (q_t) represent the amount of dye adsorbed (mg/g) at equilibrium and at time t (min), respectively, and k1 (min-1) is the equilibrium rate constant of the pseudo-first-order reaction. The measurements for the (k_1) rate constant and the (q_e(cal)) equilibrium adsorption capacity may be found using the slope and intercept of the linear lines that depict the adsorption data. At various dye concentrations, the representative graphs of Ln (q_e - q_t) versus t within an aquatic solution are given in Figure 16a.

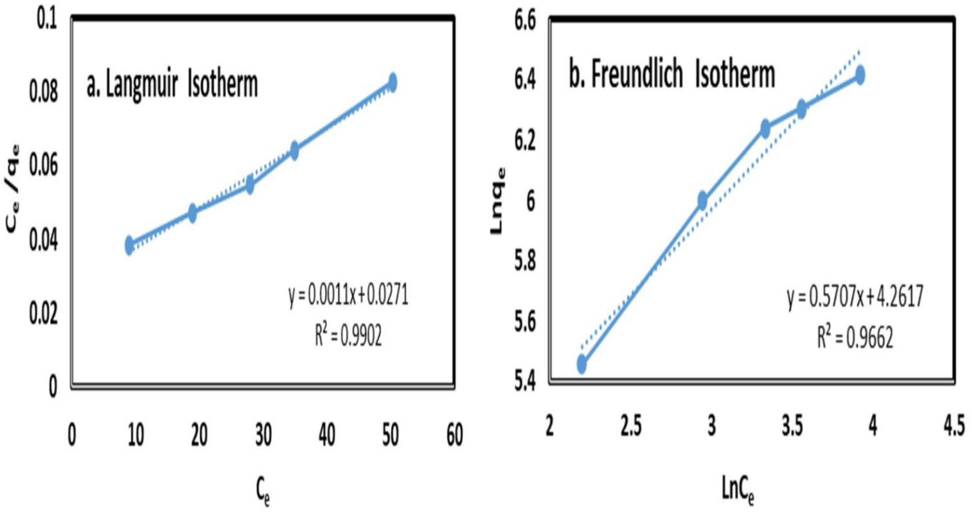

Figure 15: a. The Langmuir and b. The Freundlich isotherms of RR 12 by Fe^{3+}doped TiO_2 nanoparticles.

3.4.2. Kinetic model of the second order

Equations 22 and 23 are utilized for additional analysis of kinetic information using a pseudo-second-order kinetic approach [41].

$$\frac{t}{q_t} = \frac{1}{k_2 q_e^2} + \frac{t}{q_e} \qquad \text{Eq. (22)}$$

$$h = k_2 q_e \qquad \text{Eq. (23)}$$

If pseudo-second-order kinetics are required, a plot of t/qt against t reveals a linear connection, where k_2, mg^{-1} min^{-1}, is the pseudo-second-order adsorption rate constant at equilibrium. The plot of the second-order model's linear shape at different dye concentrations is displayed in Figure 16b and Table 7. The graph's slopes and intercepts are used to calculate the k_2 and q_e(cal).In comparison to the first-order rate kinetics approach, the second-order rate kinetics model has greater R^2 correlation coefficients. There is excellent concordance between the experimental (q_e (exp)) data and the calculated (q_e (cal)) result (Table 7).

Thus, this research indicated the existence of pseudo-second-order adsorption kinetics more accurately represented by the kinetic model, indicating a potential chemisorption mechanism for the adsorption procedure. With the transfer of electrons between RR 12 and the adsorbent, it is more probable to be predicted that the action of adsorption will include valence forces [42].

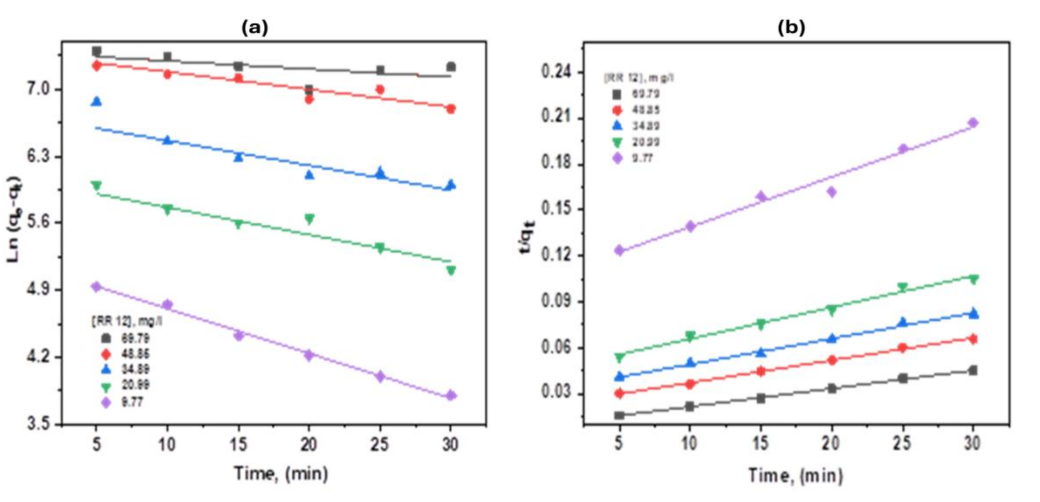

Figure16: (a) Pseudo-first-order and (b) Pseudo-second-order kinetics for adsorption of RR 12 at different concentrations by Fe^{3+}doped TiO_2 nanoparticles.

Table 7: Adsorption kinetics of RR 12 by Fe^{3+}doped TiO_2nanoparticles at varying concentrations: pseudo-first order and pseudo-second-order kinetics constants, as well as computed and experimental q_e quantities.

[RR 12], (mg/l)	q_e (exp) mg /g	Pseudo-first order			Pseudo-second order			
		k_1 min^{-1} $x10^{-3}$	q_e (cal) mg g	R^2	k_2 (g/mg min) $x10^{-5}$	q_e (cal) mg /g	h	R^2
69.79	630	10.01	1881	0.889	4.25	653	0.01	0.998
48.85	536	14.11	1339	0.934	6.11	555	0.03	0.996
34.89	512	25.02	992	0.948	7.59	507	0.03	0.993
20.93	403	30.11	304	0.968	9.89	434	0.04	0.987
9.77	224	40.05	194	0.993	19.70	285	0.05	0.974

4. Conclusion

Using a dosing amount of Fe^{3+} = 0.02 wt.%, Fe^{3+}doped TiO_2composite nanoparticles are efficiently produced using a newly developed wet impregnation approach. The produced nanoparticles were characterized using TEM, EDX, XRD, and SEM.The results demonstrate that the amount of Fe^{3+} doping decreases the TiO_2 nanoparticles' sizes. The use of doping (Fe^{3+}) can control the transition of TiO_2 from anatase to rutile and widen the dimension of the TiO_2 diffract peaks. Importantly, an appropriate doping of Fe^{3+} (approximately 0.02% in our test) can enhance the catalytic efficiency of TiO_2 in UV (ultraviolet) illumination.In the photocatalytic and photo-Fenton oxidation reactions, the Fe^{3+} doped TiO_2 catalyst degraded RR 12. Several variables can influence whether dyes break down, namely pH, catalyst, dye amount, and H_2O_2 content. When Fe^{3+} ions are added to TiO_2 nanoparticles, the rate of photo-generated hole-electron recombine decreases.Fe^{3+} doped TiO_2 is *anticipated* to be employed as an effective photocatalyst in naturally occurring cleaning domains for the degradation of organic pollution and the cleanup of aqueous contaminants, especially dye-related ones. To investigate Reactive Red 12's adsorption onto Fe^{3+}doped TiO_2 in aqueous solution.The usefulness of the Langmuir isotherm suggests that the catalyst nanoparticle surface has only one coating covering RR 12. The kinetic examinations of the process of adsorption revealed that the pseudo-second-order kinetic model was a more precise imitation of the adsorption kinetics, suggesting that the procedure for adsorption may involve chemisorption.

5. Conflicts of Interest

This is not applicable.The author was solely responsible for this study.

6. Funding

This is no funding.

7. Acknowledgments

The author thanks the reviewers for their contributions to this manuscript.

8. References

[1] Khatri J., Nidheesh P.V., Anantha SinghT.S., Suresh K. M., Advanced oxidation processes based on zero-valent aluminium for treating textile wastewater. Chem. Eng. J., 348 (2018) 67–73. https://doi.org/10.1016/j.cej.2018.04.074

[2] Imran M., Crowley D.E., Khalid A., Hussain S., Mumtaz M.W., Arshad M., Microbial biotechnology for decolorization of textile wastewaters. Rev. Environ. Sci. Bio/Technol., 14 (2015) 73–92. https://doi.org/10.1007/s11157-014-9344-4

[3] Hassan M.M., Carr C.M., A critical review on recent advancements of the removal of reactive dyes from dyehouse effluent by ion-exchange adsorbents. Chemosphere, 209 (2018) 201–219. https://doi.org/10.1016/j.chemosphere.2018.06.043

[4] Lellis B., Favaro-Polonio C.Z., Pamphile J.A., Polonio J.C., Effects of textile dyes on health and the environment and bioremediation potential of living organisms.Biotechnol, Res. Innov., 3 (2019) 275–290. https://doi.org/10.1016/j.biori.2019.09.001

[5] GhalkhaniM., Zare N., Karimi F., Karaman C., Alizadeh M., Vasseghian Y., Recent advances in Ponceau dyes monitoring as food colorant substances by electrochemical sensors and developed procedures for their removal from real samples.Food Chem. Toxicol., 161 (2022) 112830. https://doi.org/10.1016/j. fct.2022.112830

[6] Zeinab A. Suliman,Achisa C. Mecha c, Josphat I. Mwasiagi, Effect of TiO_2/Fe_2O_3nanopowder synthesis method on visible light photocatalytic degradation of reactive blue dye.Heliyon, 10 (2024) 29648. https://doi.org/10.1016/j.heliyon.2024.e29648

[7] Nadeem K., Guyer G.T., Keskinler B., Dizge N., Investigation of segregated wastewater streams reusability with membrane process for textile industry. J. Clean. Prod., 228 (2019) 1437–1445. https://doi.org/10.1016/j.jclepro.2019.04.205

[8] Wei J., Zhang Y., Zhou Z., Bi F., Qiao R., Jiang S., Wang J., Zhang X., PVP- modified spindle-shaped MIL-88B(Fe) to enhance the degradation of tetracycline by activated peroxodisulfate: a comparative study and mechanistic investigation. Prog. Nat. Sci. Mater. Int., 33 (2023) 872–880. https://doi.org/10.1016/j.pnsc.2023.12.020

[9] SamianifardS.M., Kalaee M., Moradi O., Mahmoodi N.M., Zaarei D., Synthesis of novel Starch/zeolitic imidazolate framework (ZIF-67)/Graphene oxide biocomposite and photocatalytic dye degradation ability. Opt. Mater., 151 (2024) 115268. https://doi.org/10.1016/j.optmat.2024.115268

[10] SenguttuvanS., Janaki V., Senthilkumar P., Kamala-Kannan S., Polypyrrole/ zeolite composite – a nanoadsorbent for reactive dyes removal from synthetic solution.Chemosphere, 287(2022) 132164. https://doi.org/10.1016/j. chemosphere.2021.132164

[11] Selim M.T., Salem S.S., Mohamed A.A., El-Gamal M.S., Awad M.F., Fouda A., Biological treatment of real textile effluent using Aspergillus flavus and Fusarium oxysporium and their consortium along with the evaluation of their phytotoxicity. J. Fungi, 7 (2021) 193. https://doi.org/10.3390/jof7030193.

[12] Crini G., Lichtfouse E., Advantages and disadvantages of techniques used for wastewater treatment. Environ. Chem. Lett., 17 (2019) 145–155. https://doi.org/10.1007/ s10311-018-0785-9.

[13] Gao B., Feng X., Zhang Y., Zhou Z., Wei J., Qiao R., Bi F., Liu N., Zhang X., Graphene-based aerogels in water and air treatment: a review. Chem. Eng. J., 484 (2024) 149604.https://doi.org/10.1016/j.cej.2024.149604

[14] Kim Jin-Hee, Lee Hyun-Kyu, Park Yoon-Ji, Lee Sae-Binna, Choi Sang-June, Oh Wonzin, et al. Studies on decomposition behavior of oxalic acid waste by UVC photo-Fenton Advanced Oxidation Process. Nucl Eng Technol (2019).

[15] Haider Adawiya J, Al-Anbari Riyad Hassan, Kadhim Ghadah Rasim, Salame Chafic Touma. Exploring potential environmental applications of TiO_2 nanoparticles. Energy Procedia,119(2017)332–45.

[16] Pongsert S., Witthaya K., Pornsawan A., Investigation of important parameters for Photo-Fenton degradation of methyl orange over Fe/TiO_2 catalyst. Energy Reports, 6 (2020) 731–736.

[17] Alaa A.M, Ali A. A., Hadi S. Al., Chemical Functionalization Graphene Oxide for The Adsorption Behavior of Bismarck Brown Dye from Aqueous Solutions. Egyptian Journal of Chemistry, 63 (2020) 1679 - 1696.

[18]Rojviroon O., Rojviroon T., Photocatalytic process augmented with micro/nano bubble aeration for enhanced degradation of synthetic dyes in wastewater.Water Resosur. Ind., 27 (2022) 100169.

[19] Mai M., Abdallah F. Z., Gehad G. M., Gamal K. H., Fabrication of nitrogen doped TiO_2/Fe_2O_3 nanostructures for photocatalytic oxidation of methanol based wastewater.Nature, 13 (2023)4431.

[20] Naeem K., Ouyang F., Preparation of Fe^{3+}-doped TiO_2 nanoparticles and its photocatalytic activity under UV light. Physica B, 405 (2010) 221–226.

[21] Zhu Y., Zeng C., Zhu R., Xu Y., Wang X., Zhou H., TiO_2/Schwert mannite nanocomposites as superior co-catalysts in heterogeneous photo-Fenton process.J Environ Sci, 80(2019)208–17.

[22] Zhu Y., Zhu R., Yan L., Fu H., Xi Y., Zhou H.,Visible-light Ag/AgBr/ferrihydrite catalyst with enhanced heterogeneous photo-Fenton reactivity via electron transfer from Ag/AgBr to ferrihydrite. Appl Catal B, 239(2018)280–9.

[23] Chen F., Huang H., Zhang Y., Zhang T., Achieving UV and visible-light photocatalytic activity enhancement of gI/$BiOIO_3$ heterostructure: Decomposition for diverse industrial contaminants and high mineralization ability. Chin Chem Lett, 28 (2017) 2244–50.

[24] Adil R., Honglie S., Azhar A.H., Shusong C., Hydrothermal synthesis of $Fe_3O_4/TiO_2/g\text{-}C_3N_4$: Advanced photocatalytic application. Applied Surface Science, 488 (2019) 887–895.

[25] Xu L., Meng L., Zhang X., Mei X.,Guo X., Li W., Wang P., Gan L., Promoting Fe^{3+}/Fe^{2+} cycling under visible light by synergistic interactions between P25 and small amount of Fenton reagents. J. Hazard. Mater., 379 (2019) 120795.

[26] Behzad R., Nayereh R., Afshin E., Catalytic reduction of hazardous acid orange 10 dye by $BiVO_4/TiO_2$ nanocrystalline heterojunction and influence of aeration, $FeSO_4$, H_2O_2 and $FeCl_3$ on removal efficiency: A novel and environmentally friendly process. Arabian Journal of Chemistry 15 (2022) 104003.

[27] Fujishima A., Zhang X., Titanium dioxide photocatalysis: present situation and future approaches. Compt. Rendus Chem., 9 (5) (2006) 750–760.

[28] Fangfei L., Shenmei S., Yinshan J., Maosheng X., Mengmeng S., Bing X., Photodegradation of an azo dye using immobilized nanoparticles of TiO_2 supported by natural porous mineral. J. Hazard Mater., 152 (2008) 1037–1044.

[29]Ramimoghadam D., Bagheri S., Abd Hamid S.B., Biotemplated synthesis of anatase titanium dioxide nanoparticles via lignocellulosic waste material. BioMed Res. Int., (2014).

[30]Pragathiswaran C., Smitha C., Mahin B., Govindhan P., Anantha N., Synthesis and characterization of TiO_2/ZnO–Ag nanocomposite for photocatalytic degradation of dyes and anti-microbial activity.Mater. Today: Proc., 45 (2021) 3357–3364.

[31] Mathews R.W., Purification of water with near-UV illuminated suspensions of titanium dioxide. Water Research, 24 (1990) 653-660.

[32] Mohamed A. Ben A., Khairy M., Magdi E. K., Ehab A. A., Nadeem R., Emad M. M., Abueliz M., Facile synthesis of TiO_2at ZnO nanoparticles for enhanced removal of methyl orange and indigo carmine dyes: Adsorption, kinetics.Heliyon, 10 (2024) 31351.

[33] Chiou C. H., Wu C. Y., Juang R. S., Influence of operating parameters on photocatalytic degradation of phenol in UV/TiO_2 process. Chem. Engin. J., 139 (2008) 322-329.

[34] Uddin M. D., Islam M. D., Mahmud S., Rukanuzzaman M. d., Adsorptive removal of methylene blue by tea waste.Journal of Hazardous Materials, 164 (2009) 53–60. https://doi.org/10.1016/j.jhazmat.2008.07.131

[35] Alaa M.M., Collaborative impact of Cu/TiO_2 nano composites for elimination of cationic dye from aqueoussolution: Kinetics and isothermal modeling. Arabian Journal of Chemistry,16 (2023) 104815. https://doi.org/10.1016/j.arabjc.2023.104815

[36] Khezami L., Modwi A., Ghiloufi I., Taha K.K., Bououdina M., ElJery A., El Mir L., Effect of aluminum loading on structural and morphological characteristics of ZnO nanoparticles for heavy metal ion elimination. Environ. Sci. Pollut. Control Ser., 27 (2020) 3086–3099. https://doi.org/10.1007/s11356-019-07279-0

[37] Khalfaoui A., Meniai A. H., Derbal K., Isotherm and Kinetics Study of Biosorption of Cationic Dye onto Banana Peel. Energy Procedia, 19 (2012) 286 – 295.

[38] Ahmed Y.H., Salah H.M., Ahlaam M.Y., Kinetic Study for some effects on auto-catalyzed oxidation for Serine, Thrionine and Tyrosene Egyptian Journal of Chemistry,66 (2023) 507 – 515.

[39] Hany G., Optimization of the Process Factors Affecting Extraction of Uranium from Acidic Solution Using Activated Carbon and Kinetics Studies of the adsorption Process. Egyptian Journal of Chemistry, 64 (2021) 1743 - 1750.

[40] Al-Bizreh W.Y., Al-mostafa R., AL-Joubbeh M., Adsorption of Nicotine on Calcinated and Modified Compressed Coffee Residue CACS and Its Surface Properties. Egyptian Journal of Chemistry, 61 (2018) 1083 - 1096 .

[41] RobatiD., Pseudo-second-order kinetic equations for modeling adsorption systems for removal of lead ions using multi-walled carbon nanotube. Journal of Nanostructure in Chemistry, 3 (2013) 55.

[42] Behnajady M.A., Modirshahla N., Hamzavi R., Kinetic study on photocatalytic degradation of C.I. Acid Yellow 23 by ZnO photocatalyst.Journal of Hazardous Materials, B133 (2006) 226–232. https://doi.org/10.1016/j.jhazmat.2005.10.022